Acta Crystallographica Section B
Structural Science
ISSN 0108-7681

Helical screw type magnetic structure of the multiferroic $CaMn_7O_{12}$ with low Cu-doping

W. Sławiński,[a]* R. Przeniosło,[a] I. Sosnowska[a] and V. Petříček[b]

[a]Institute of Experimental Physics, University of Warsaw, 00-681 Warsaw, Hoża 69, Poland, and [b]Institute of Physics of the Academy of Sciences of the Czech Republic, v.v.i., Na Slovance 2, 182 21 Praha 8, Czech Republic

Correspondence e-mail: wojciech.slawinski@fuw.edu.pl

Received 8 September 2011
Accepted 22 February 2012

The modulated crystal structure and modulated magnetic ordering of the multiferroic $CaCu_xMn_{7-x}O_{12}$ is studied by analysing neutron and synchrotron-radiation (SR) powder diffraction data with a model based on the magnetic superspace group $R31'(00\gamma)ts$. Both atomic position modulations and magnetic modulations are described with the modulation vector $(0, 0, q)$. The magnetic ordering is a screw-type circular helix where the magnetic moments are perpendicular to the **c** direction. The temperature dependence of the modulation vector length and the ordered magnetic moments of Mn^{3+} and Mn^{4+} ions is given between $T = 50$ K and the Néel temperature $T_N \simeq 90$ K. The atomic position modulation length L_p and the magnetic modulation length L_m fulfil the relation $L_m = 2L_p$ at all temperatures between 50 K and T_N.

1. Introduction

The coupling of the spin, charge and lattice degrees of freedom is an important phenomenon which determines the physical properties of transition metal oxides (Dagotto *et al.*, 2001). These properties include magnetoelectric and magnetoelastic effects (Fiebig, 2005; Wang *et al.*, 2009) as well as colossal magnetoresistance and colossal dielectric constants (Lunkenheimer *et al.*, 2010). Several studies have shown that a relation exists between the modulated magnetic ordering and the magnetoelectric coupling (Katsura *et al.*, 2005; Mostovoy, 2006) as observed in several materials, *e.g.* $BiFeO_3$ (Sosnowska *et al.*, 1982; Lee *et al.*, 2008), CuO (Kimura *et al.*, 2008), $TbMnO_3$ (Yamasaki *et al.*, 2007) and YMn_2O_5 (Kim *et al.*, 2008).

$CaCu_xMn_{7-x}O_{12}$ belongs to a distorted perovskite family (Vasiliev & Volkova, 2007). These materials show magnetoelectric coupling (Sánchez-Andújar *et al.*, 2009) with considerably large values for the electric polarization (Zhang *et al.*, 2011; Johnson *et al.*, 2012), modulation of the atomic positions (Sławiński *et al.*, 2009), modulations of the magnetic ordering (Sławiński *et al.*, 2009; Przeniosło *et al.*, 1999; Sławiński *et al.*, 2010) and a colossal dielectric constant (Yáñez-Vilar *et al.*, 2005). In our earlier paper (Przeniosło *et al.*, 1999) the resolution was not sufficient to observe the magnetic modulations above 50 K. There is a remarkable correlation between the onset of the atomic position modulation at 250 K in $CaMn_7O_{12}$ (Sánchez-Andújar *et al.*, 2009) and the decrease of the colossal dielectric constant by four orders of magnitude below 250 K (Yáñez-Vilar *et al.*, 2005). In addition, a correlation of the onset of the magnetoelectric coupling below 50 K and the magnetic phase transition with changes of the magnetic modulation lengths at 50 K is observed (Przeniosło *et al.*, 1999). The appearance of an atomic position modulation at

Table 1
Positions of Ca, Cu, Mn and O ions in the average $CaCu_xMn_{7-x}O_{12}$ crystal structure given in the hexagonal setting of the space group $R\bar{3}$.

The atomic position labels are the same as those used in Bochu *et al.* (1980).

Label	Ions	Position	x_h	y_h	z_h
Ca	Ca^{2+}	3*a*	0	0	0
Mn1	Mn^{3+}/Cu^{2+}	9*e*	1/2	0	0
Mn2	Mn^{3+}/Mn^{4+}	9*d*	1/2	1/2	1/2
Mn3	Mn^{4+}	3*b*	0	0	1/2
O1	O^{2-}	18*f*	x_1	y_1	z_1
O2	O^{2-}	18*f*	x_2	y_2	z_2

250 K and the magnetic phase transition at 50 K are associated with anomalies of the thermal expansion of $CaMn_7O_{12}$, as shown by powder X-ray diffraction measurements at the synchrotron (Przeniosło *et al.*, 2004; Sánchez-Andújar *et al.*, 2009) and macroscopic thermal expansion (Volkova *et al.*, 2005). Recent studies report magnetically induced ferroelectricity in $CaMn_7O_{12}$ single crystals (Zhang *et al.*, 2011; Johnson *et al.*, 2012). The magnetic ordering of $CaMn_7O_{12}$ has been recently studied using powdered single-crystal samples (Johnson *et al.*, 2012).

One of the most important indications of the magnetoelastic coupling in $CaMn_7O_{12}$ is the recent observation of the relation between the magnetic modulation length L_m and the atomic position modulation L_p (Sławiński *et al.*, 2010). Although both modulations are incommensurate with the lattice they fulfil the relation $L_m = 2L_p$ for two compositions: $CaCu_xMn_{7-x}O_{12}$, $x = 0$ and $x = 0.1$ (Sławiński *et al.*, 2010). This observation suggests that both modulations should be described with the same superspace group. This is why we present an extended symmetry analysis of our earlier synchrotron-radiation (Sławiński *et al.*, 2009) and neutron (Sławiński *et al.*, 2010) powder diffraction data.

2. Experimental

Polycrystalline samples of $CaCu_xMn_{7-x}O_{12}$ (x = 0.0, 0.1 and 0.23) were prepared from stoichiometric amounts of $CaCO_3$ (CERAC, 99.995%), CuO (CERAC, 99.999%) and Mn_2O_3 (CERAC, 99.99%) and reacted at 1223 K with KCl as a mineralizer. The synthesis details are presented in Sławiński *et al.* (2006).

We are using two sets of our neutron powder diffraction experiments carried out at the Institute Laue–Langevin (ILL), Grenoble. The high-resolution powder neutron diffractograms of $CaMn_7O_{12}$ were measured on the diffractometer D2B. The powder $CaMn_7O_{12}$ sample was placed in a Displex in a cylindrical vanadium container (15 mm diameter). Using a wavelength of 1.595 Å and a scattering angle of 2θ in the range $5.0 \leq 2\theta \leq 160.0^\circ$ diffractograms were collected at 10, 60, 100 and 290 K. A series of diffractograms for $CaCu_xMn_{7-x}O_{12}$ (x = 0.0, 0.1 and 0.23) were measured as a function of temperature by using the high-flux neutron diffractometer D20. The $CaCu_xMn_{7-x}O_{12}$ powder samples were measured in a standard orange cryostat in a cylindrical vanadium container (8 mm diameter). Powder diffraction patterns were recorded from 10 K up to 290 K using a neutron wavelength of 2.418 Å covering the scattering angle, 2θ, range $10.0 \leq 2\theta \leq 140.0^\circ$. The neutron powder diffraction patterns were analysed by the Rietveld method (Rietveld, 1969) using the *JANA*2006 (Petříček *et al.*, 2006) program.

3. Results

3.1. Crystal structure

The average crystal structure of $CaCu_xMn_{7-x}O_{12}$ is described in the literature by using the trigonal space group $R\bar{3}$ (Bochu *et al.*, 1980; Zeng *et al.*, 1999). The space group $R\bar{3}$, in the hexagonal setting, gives three $CaCu_xMn_{7-x}O_{12}$ formula units per unit cell. The atomic positions in $R\bar{3}$ space group are presented in Table 1. For undoped $CaMn_7O_{12}$ the Mn1 and Mn2 positions should contain Mn^{3+} ions only. It is important to note that the Cu^{2+} ions replace Mn^{3+} ions only in the position (9*e*) (Zeng *et al.*, 1999).

There is a modulation of the atomic positions in $CaMn_7O_{12}$ below 250 K (Sławiński *et al.*, 2009) as observed with SR diffraction data. This modulation has been quantitatively described using the non-magnetic superspace group $R\bar{3}(00\gamma')0$ with $\gamma' = 0.9203\,(1)$ at 10 K (Sławiński *et al.*, 2009). The modulation vector used was $(0, 0, q'_p)$ where $q'_p = 0.9203\,(1)$.

The magnetic ordering in $CaMn_7O_{12}$ leads to a magnetic modulated structure and which gives rise to satellite Bragg peaks in neutron powder diffraction patterns, but now indexed with the modulation vector $(0, 0, q'_m)$ where $q'_m = 0.96$ (Sławiński *et al.*, 2010).

In the present paper we present a common model which describes both these modulations by using the same superspace group with one modulation vector $(0, 0, q)$. In this model the magnetic ordering contributes to first-order satellites, while the atomic position modulation contributes to second-order satellites.

The representation analysis of the parent paramagnetic space group $R\bar{3}1'$ was made with the help of the *ISODISTORT* program developed by Stokes *et al.* (2011). This program uses an approach similar to that described in Campbell *et al.* (2006), which is also applicable to modulated magnetic structures (Perez-Mato *et al.*, 2012). The results of the analysis together with the corresponding symmetry restrictions for positional and magnetic modulation Fourier components of Mn atoms are listed in Table 2. Note that in the table all irreps leading to 'grey' magnetic superspace groups are omitted as they would not give magnetic satellites.

Our analysis shows (see §3.2) that a common model describing both modulations is obtained with the magnetic superspace group $R31'(00\gamma)ts$ based on the irrep $m\Lambda_2\Lambda_3$ for the order parameter $(a, b, 0, 0)$. The atomic position modulation for an atom i is described with second-order Fourier coefficients

$$\mathbf{r}_i = \mathbf{r}_{i0} + \mathbf{U}_{2is}\sin(4\pi x_4) + \mathbf{U}_{2ic}\cos(4\pi x_4), \qquad (1)$$

Table 2
Physically irreducible representations of the parent paramagnetic space group $R\bar{3}1'$ for the incommensurate modulation vector (00γ).

All order parameter directions (OPD), which lead to non-equivalent magnetic superspace groups, are listed together with their magnetic superspace groups and symmetry restrictions for positions of magnetic atoms. M_{1sx}, M_{1sy}, M_{1sz}, M_{1cx}, M_{1cy} and M_{1cz} denote magnetic sine and cosine Fourier coefficients (first order) along x, y and z axes, respectively, whereas U_{2sx}, U_{2sy}, U_{2sz}, U_{2cx}, U_{2cy} and U_{2cz} denote the atomic position sine and cosine Fourier coefficients (second order) along x, y and z axes, respectively.

Irrep	OPD	SSG	Mn1/Mn2			Mn3		
$m\Lambda_1$	$(a, 0)$	$R\bar{3}1'(00\gamma)0s$	0	0	0	0	0	0
			M_{1cx}	M_{1cy}	M_{1cz}	0	0	M_{1cz}
			U_{2sx}	U_{2sy}	U_{2sz}	0	0	U_{2sz}
			0	0	0	0	0	0
$m\Lambda_2\Lambda_3$	$(a, b, 0, 0)$	$R31'(00\gamma)ts$	M_{1sx}	M_{1sy}	M_{1sz}	M_{1sx}	M_{1sy}	0
			M_{1cx}	M_{1cy}	M_{1cz}	$M_{1cx} = -\frac{1}{\sqrt{3}}M_{1sx} + \frac{2}{\sqrt{3}}M_{1sy}$	$M_{1cy} = -\frac{2}{\sqrt{3}}M_{1sx} + \frac{1}{\sqrt{3}}M_{1sy}$	0
			U_{2sx}	U_{2sy}	U_{2sz}	U_{2sx}	U_{2sy}	0
			U_{2cx}	U_{2cy}	U_{2cz}	$U_{2cx} = \frac{1}{\sqrt{3}}U_{2sx} - \frac{2}{\sqrt{3}}U_{2sy}$	$U_{2cy} = \frac{2}{\sqrt{3}}U_{2sx} - \frac{1}{\sqrt{3}}U_{2sy}$	0
$m\Lambda_2\Lambda_3$	$(a, b, a, -b)$	$R\bar{1}1'(\alpha\beta\gamma)0s$	0	0	0	0	0	0
			M_{1cx}	M_{1cy}	M_{1cz}	M_{1cx}	M_{1cy}	M_{1cz}
			U_{2sx}	U_{2sy}	U_{2sz}	U_{2sx}	U_{2sy}	U_{2sz}
			0	0	0	0	0	0
$m\Lambda_2\Lambda_3$	(a, b, c, d)	$R11'(\alpha\beta\gamma)0s$	M_{1sx}	M_{1sy}	M_{1sz}	M_{1sx}	M_{1sy}	M_{1sz}
			M_{1cx}	M_{1cy}	M_{1cz}	M_{1cx}	M_{1cy}	M_{1cz}
			U_{2sx}	U_{2sy}	U_{2sz}	U_{2sx}	U_{2sy}	U_{2sz}
			U_{2cx}	U_{2cy}	U_{2cz}	U_{2cx}	U_{2cy}	U_{2cz}

Table 3
Symmetry operators for the magnetic superspace group $R31'(00\gamma)ts$.

The symbol $-m$ means time inversion, while m means no time inversion. The position coordinates x_1, x_2, x_3 are given in the hexagonal system (see Table 1).

E	x_1	x_2	x_3	x_4	m
3	$-x_2$	$x_1 - x_2$	x_3	$x_4 + \frac{1}{3}$	m
3^2	$-x_1 + x_2$	$-x_1$	x_3	$x_4 + \frac{2}{3}$	m
$E(1'\|000\frac{1}{2})$	x_1	x_2	x_3	$x_4 + \frac{1}{2}$	$-m$
$3(1'\|000\frac{1}{2})$	$-x_2$	$x_1 - x_2$	x_3	$x_4 + \frac{5}{6}$	$-m$
$3^2(1'\|000\frac{1}{2})$	$-x_1 + x_2$	$-x_1$	x_3	$x_4 + \frac{1}{6}$	$-m$

Table 4
Symmetry operators for the magnetic superspace group $R31'(00\gamma)0s$.

The symbol $-m$ means time inversion, while m means no time inversion. The position coordinates x_1, x_2, x_3 are given in the hexagonal system (see Table 1).

E	x_1	x_2	x_3	x_4	m
3	$-x_2$	$x_1 - x_2$	x_3	x_4	m
3^2	$-x_1 + x_2$	$-x_1$	x_3	x_4	m
$E(1'\|000\frac{1}{2})$	x_1	x_2	x_3	$x_4 + \frac{1}{2}$	$-m$
$3(1'\|000\frac{1}{2})$	$-x_2$	$x_1 - x_2$	x_3	$x_4 + \frac{1}{2}$	$-m$
$3^2(1'\|000\frac{1}{2})$	$-x_1 + x_2$	$-x_1$	x_3	$x_4 + \frac{1}{2}$	$-m$

where $\mathbf{U}_{2is}$ and $\mathbf{U}_{2ic}$ denote the sine and cosine Fourier second-order coefficients, $x_4 = \mathbf{q}_m(\mathbf{r}_{i0} + \mathbf{T})$ is an internal coordinate and $\mathbf{T}$ is a lattice translation of the average crystal structure.

The magnetic moment of the atom i located at position r_i in the unit cell is expressed with first-order Fourier terms as

$$\mathbf{M}_i = \mathbf{M}_{i0} + \mathbf{M}_{is}\sin(2\pi x_4) + \mathbf{M}_{ic}\cos(2\pi x_4), \qquad (2)$$

where $\mathbf{M}_{is}$ and $\mathbf{M}_{ic}$ denote the sine and cosine Fourier first-order coefficients. The constant (non-modulated) contribution $\mathbf{M}_{i0} = 0$ for all magnetic ions in the case of $CaCu_xMn_{7-x}O_{12}$ compounds as follows from the presence of the superspace symmetry operator $(1'|0, 0, 0, 1/2)$.

In the present model the modulation vector $(0, 0, q)$ is used which is related to the modulation vector $(0, 0, q_p')$ used earlier in Sławiński *et al.* (2009) by the relation

$$q = \frac{1}{2}(3 - q_p'). \qquad (3)$$

In the present model the magnetic satellites are indexed as $q_m = q = 1 + \delta \simeq 1.0398$ (first order), while the satellites due to atomic position modulations are indexed with $q_p = 2q = 2 + 2\delta \simeq 2.0796$ (second order).

The atomic modulation observed in $CaMn_7O_{12}$ at 70 K (SR diffraction data) has been refined with the present model (superspace group $R31'(00\gamma)ts$) and the previous model (superspace group $R\bar{3}1'(00\gamma)0s$) as described in Sławiński *et al.* (2009). The symmetry operators for both superspace groups are given in Tables 3 and 4 (Petříček *et al.*, 2010). The atomic position modulation amplitudes determined with both models are shown in Table 5.

Both models give different modulations, but the refinement quality estimators are similar. Please note that the amplitudes determined in the previous model with $R\bar{3}1'(00\gamma)0s$ ($T = 70$ K) are not the same as those given in Sławiński *et al.* (2009) for $T = 10$ K (different temperatures).

3.2. Magnetic ordering

The neutron powder diffraction pattern of $CaMn_7O_{12}$ observed at 60 K could be satisfactorily described using the superspace group $R31'(00\gamma)ts$. This magnetic ordering model will be denoted as the *circular model* because the magnetic moments show a screw-type modulated ordering.

3.2.1. Circular model of magnetic ordering. The magnetic superspace group $R31'(00\gamma)ts$ implies the following restriction on the Fourier coefficients of Mn^{4+} magnetic moments located at the $3b$ position

Table 5
Atomic position modulation amplitudes obtained from SR powder diffraction pattern refinements of $CaMn_7O_{12}$ at 70 K with the present model (superspace groups $R31'(00\gamma)ts$) and the previous model (superpsace group $R31'(00\gamma)0s$).

The lattice modulation contributes to the second-order satellites of the modulation vector [0, 0, 1.03985 (1)].

	Present model: $R31'(00\gamma)ts$			Previous model: $R31'(00\gamma)0s$		
	x U_{2sx} U_{2cx}	y U_{2sy} U_{2cy}	z U_{2sz} U_{2cz}	x U_{2sx} U_{2cx}	y U_{2sy} U_{2cy}	z U_{2sz} U_{2cz}
Ca	0	0	0	0	0	0
	0.0076 (8)	0.0096 (11)	0	0	0	−0.0108 (13)
	0.0066 (0)	−0.0033 (0)	0	0	0	0
Mn1	0.5	0	0	0.5	0	0
	0.0018 (6)	−0.0078 (5)	0.0030 (8)	0.0108 (2)	−0.0047 (3)	0.0093 (4)
	0.0056 (6)	0.0034 (8)	0.0045 (7)	0	0	0
Mn2	0.5	0.5	0.5	0.5	0.5	0.5
	−0.0007 (6)	−0.0020 (7)	0.0027 (6)	0.0061 (2)	0.0049 (3)	−0.0030 (6)
	0.0026 (7)	−0.0016 (6)	0.0000 (10)	0	0	0
Mn3	0	0	0.5	0	0	0.5
	−0.0038 (6)	−0.0041 (8)	0	0	0	0.0082 (10)
	−0.0025 (0)	0.0020 (0)	0	0	0	0
O1	0.2236 (3)	0.2740 (3)	0.0814 (4)	0.2236 (3)	0.2741 (3)	0.0816 (4)
	−0.0074 (8)	−0.0048 (8)	0.0022 (15)	0.0066 (7)	0.0076 (7)	−0.0003 (12)
	0.0033 (7)	−0.0028 (9)	0.0006 (16)	0.0016 (8)	0.0060 (7)	−0.0027 (7)
O2	0.3416 (3)	0.5218 (3)	0.3407 (4)	0.3420 (3)	0.5221 (3)	0.3415 (4)
	0.0006 (7)	−0.0030 (8)	0.0087 (15)	0.0061 (7)	0.0001 (7)	0.0080 (12)
	0.0004 (11)	−0.0009 (13)	0.0046 (14)	−0.0032 (10)	−0.0006 (9)	−0.0100 (12)
Refinement agreement factors	wR(all)		6.69	wR(all)		6.42
	wR(all) for main		5.39	wR(all) for main		4.49
	R(obs) for satellites		9.09	R(obs) for satellites		8.14
	wR(obs) for satellites		8.28	wR(obs) for satellites		7.73
	R(all) for satellites		11.21	R(all) for satellites		9.26
	wR(all) for satellites		8.71	wR(all) for satellites		7.79
	GOF		1.84	GOF		1.89
	Rwp		23.22	R_{wp}		23.92

$$M_{1cx}[\mathrm{Mn3}] = \frac{2}{\sqrt{3}} M_{1sy}[\mathrm{Mn3}] - \frac{1}{\sqrt{3}} M_{1sx}[\mathrm{Mn3}] \quad (4)$$

$$M_{1cy}[\mathrm{Mn3}] = \frac{1}{\sqrt{3}} M_{1sy}[\mathrm{Mn3}] - \frac{2}{\sqrt{3}} M_{1sx}[\mathrm{Mn3}] \quad (5)$$

$$M_{1cz}[\mathrm{Mn3}] = 0 \quad M_{1sz}[\mathrm{Mn3}] = 0. \quad (6)$$

These restrictions imply that the $\mathbf{M}_{1s}$[Mn3] and $\mathbf{M}_{1c}$[Mn3] vectors are perpendicular to each other and they have the same length so they describe a screw-type circular ordering. The amplitudes of magnetic moments for the Mn^{3+} ions at Mn1 and Mn2 positions are not restricted as these atoms occupy the general positions 9*e* and 9*d*. However, from testing refinements we found that the circular model imposed on all magnetic atoms gives a very reasonable fit and a stable refinement. For this reason we applied the same restrictions 4,5,6 to the Fourier coefficients of magnetic moments of atoms Mn1 (9*e*) and Mn2 at (9*d*). Owing to the fact that the magnetic superspace group $R31'(00\gamma)ts$ is polar the phase of one helicoid has to be fixed and there are only two free relative phases. The modulation vector length q_m together with the three independent magnetic amplitudes for Mn1, Mn2 and Mn3 give six refineable parameters.

The Cu^{2+} ions replace a small amount of the Mn ions at 9*e* positions and not in the remaining 9*d* or 3*b* positions of the space group $R\bar{3}$ (see Table 1). One can assume that the ordered magnetic moments for ions on the 9*e* positions may differ from those on the 9*d* positions for doped $CaCu_xMn_{7-x}O_{12}$ ($x>0$). Refinement with different magnetic moment amplitudes was performed and the agreement factors did not improve with respect to those obtained with equal magnetic moment amplitudes for Mn1 and Mn2. One can conclude that the relatively low Cu doping (with Cu/Mn = 0.23/2.77 for x = 0.23) does not lead to different ordered magnetic moments at the 9*d* and 9*e* positions.

The refinement of the magnetic structure with the five magnetic parameters mentioned above shows no significant difference between the magnetic amplitudes of the Mn1 and Mn2 atoms. Moreover, the relative phases Mn2/Mn1 and Mn3/Mn1 are not significantly different from π and 0. In the final model of the circular model only two magnetic amplitudes, M_1 and M_3, were refined. This is closely related to the fact that positions of the magnetic atoms, as reported in Table 1, make a sublattice having the space group $R\bar{3}2$.

$$M_{1cx}[\mathrm{Mn1}] = M_1 \quad M_{1cy}[\mathrm{Mn1}] = 0 \quad (7)$$

$$M_{1sx}[\mathrm{Mn1}] = \frac{M_1}{\sqrt{3}} \quad M_{1sy}[\mathrm{Mn1}] = \frac{2M_1}{\sqrt{3}}. \quad (8)$$

The same conditions for the magnetic moments of the Mn3 atom are

$$M_{1cx}[\mathrm{Mn3}] = M_3 \quad M_{1cy}[\mathrm{Mn3}] = 0 \quad (9)$$

Table 6
List of the magnetic ions positions in $CaCu_xMn_{7-x}O_{12}$.

The columns 'cosine' and 'sine' denote the Fourier coefficients [see equation (2)] to be used to refine neutron powder diffraction data within the *circular model*. Parameters M_1 and M_3 are independently refined.

Label	Position	First atom	Ion	'Cosine'	'Sine'
Mn1	9*e*	$\frac{1}{2}, 0, 0$	Mn^{3+}	M_1	M_1
Mn2	9*d*	$\frac{1}{2}, \frac{1}{2}, \frac{1}{2}$	Mn^{3+}	$-M_1$	$-M_1$
Mn3	3*b*	$0, 0, \frac{1}{2}$	Mn^{4+}	M_3	M_3

$$M_{1sx}[\mathrm{Mn3}] = \frac{M_3}{\sqrt{3}} \quad M_{1sy}[\mathrm{Mn3}] = \frac{2M_3}{\sqrt{3}}. \tag{10}$$

The result is summarized in Table 6. The fact that the magnetic moments of Mn2 are antiparallel to those of Mn1 is expressed by the additional phase factor $e^{i\pi}$. It is worthwhile mentioning that the used model gives a regular ordering of magnetic moments in the column Mn2/Mn3 (see Fig. 1).

By using the notation used in *BasiReps* and *FULLPROF* programs (Rodríguez-Carvajal, 1993) the Fourier components of the *circular model* are given as

$$\mathbf{M}_{1c}[\mathrm{Mn1}] = \mathrm{Re}(u_1, v_1, w_1) \quad \mathbf{M}_{1s}[\mathrm{Mn1}] = \mathrm{Im}(u_1, v_1, w_1) \tag{11}$$

$$\mathbf{M}_{1c}[\mathrm{Mn3}] = \mathrm{Re}(u_3, v_3, w_3) \quad \mathbf{M}_{1s}[\mathrm{Mn3}] = \mathrm{Im}(u_3, v_3, w_3) \tag{12}$$

where u_1, v_1, w_1 and u_3, v_3, w_3 are complex numbers.

The superspace group $R31'(00\gamma)ts$ leads to the conditions [see equations (4)–(10)]

$$u_1 = M_1\left(1 + \frac{i}{\sqrt{3}}\right) \quad v_1 = M_1\frac{2i}{\sqrt{3}} \quad w_1 = 0 \tag{13}$$

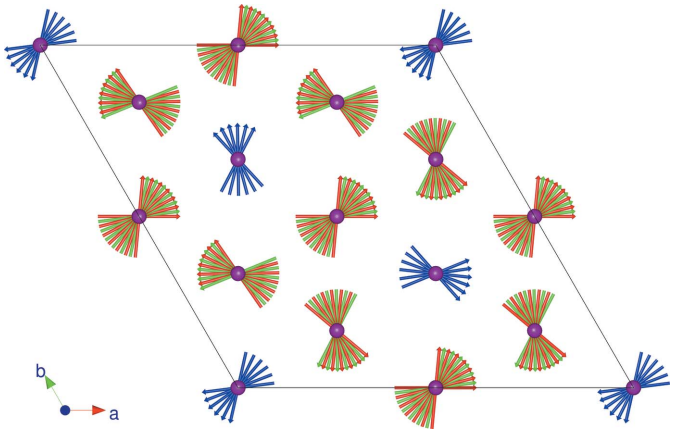

Figure 1
Schematic representation of the circular magnetic ordering in $CaMn_7O_{12}$ (view of six unit cells along the modulation vector direction, *i.e.* the *c*-axis). The red and green arrows represent the magnetic moments of Mn^{3+} ions located in the Mn1 and Mn2 sublattices. The nearest neighbours (along *c*) in the Mn1 and Mn2 sublattices are distant by $c/2$ (see Table 7). The blue arrows represent the magnetic moments of Mn^{4+} ions located in the Mn3 sublattice. The nearest neighbours (along **c**) in the Mn3 sublattice are distant by *c*. This figure is in colour in the electronic version of this paper.

$$u_3 = M_3\left(1 + \frac{i}{\sqrt{3}}\right) \quad v_3 = M_3\frac{2i}{\sqrt{3}} \quad w_3 = 0, \tag{14}$$

where M_1 and M_3 are positive real parameters [defined by equations (7)–(10)] equal to the values of the ordered magnetic moment for Mn^{3+} and Mn^{4+} ions, respectively.

The values of the Fourier components for all the Mn^{3+} and Mn^{4+} atomic positions in the hexagonal $CaMn_7O_{12}$ unit cell are given in Tables 6 and 7 (column: *circular model*) and shown in Fig. 2 as well as in Fig. 8 in the supplementary material.[1] The magnetic moment values can be calculated using equations (2), (11) and (12) for the $(u_1, v_1, 0)$ and $(u_3, v_3, 0)$.

The lattice translation of rhombohedral centring by $(\frac{2}{3}, \frac{1}{3}, \frac{1}{3})$ is associated with a turn of the magnetic moment direction by $\frac{2\pi}{3}q_m \simeq 124.7^\circ$. The translation by $(\frac{1}{3}, \frac{2}{3}, \frac{2}{3})$ is associated with a turn of the magnetic moment direction by $\frac{4\pi}{3}q_m \simeq 249.4^\circ$.

The *circular model* of the magnetic ordering described above gives a satisfactory agreement with the neutron powder diffraction data obtained for $CaCu_xMn_{7-x}O_{12}$, $x = 0$, 0.1 and 0.23, at temperatures between 50 K and T_N. The details of the refinements will be given in §3.2.2.

3.2.2. Elliptical model of magnetic ordering. There is another family of modulated magnetic ordering models (denoted as *elliptical models*), which give the same agreement with neutron powder diffraction data as the *circular model*. These *elliptical models* cannot be described by using the first two magnetic superspace groups listed in Table 2. The *elliptical model* orderings are compatible with the magnetic superspace group $R11'(\alpha\beta\gamma)0s$. The magnetic Fourier components for the *elliptical model* are given in Table 7 and the magnetic-moment directions are shown in Fig. 2.

The magnetic moments rotate within ellipses that lie at constant *z*-planes. It is assumed that the ellipse main axis is turned by the α angle with respect to the hexagonal *a* axis. For the Mn2 atom the magnetic-moment Fourier component vectors are given as

$$u_1 = A_1\left[\cos\alpha + \frac{1}{\sqrt{3}}\sin\alpha\right] + iB_1\left[-\sin\alpha + \frac{1}{\sqrt{3}}\cos\alpha\right] \tag{15}$$

$$v_1 = A_1\left[\frac{2}{\sqrt{3}}\sin\alpha\right] + iB_1\left[\frac{2}{\sqrt{3}}\cos\alpha\right] \tag{16}$$

$$w_1 = 0. \tag{17}$$

For the Mn3 atom the magnetic moment Fourier component vectors are given as

$$u_3 = A_3\left[\cos\alpha + \frac{1}{\sqrt{3}}\sin\alpha\right] + iB_3\left[-\sin\alpha + \frac{1}{\sqrt{3}}\cos\alpha\right] \tag{18}$$

$$v_3 = A_3\left[\frac{2}{\sqrt{3}}\sin\alpha\right] + iB_3\left[\frac{2}{\sqrt{3}}\cos\alpha\right]. \tag{19}$$

[1] Supplementary data for this paper are available from the IUCr electronic archives (Reference: PZ5097). Services for accessing these data are described at the back of the journal.

Table 7
Atomic positions of Mn^{3+} and Mn^{4+} ions in the $CaMn_7O_{12}$ unit cell.

The (x, y, z) coordinates are given in the hexagonal setting of the space group $R\bar{3}$. The magnetic moment Fourier components for the *circular model* are described within the superspace group $R31'(00\gamma)ts$ and the irreducible representation $m\Lambda_2\Lambda_3$ (see Table 2). The magnetic moment Fourier components for the *elliptical model* are described within the superspace group $R11'(\alpha\beta\gamma)0s$. The complex parameters u_1, v_1, u_3, v_3 are restricted by equations given in the header of each column.

	Atomic position	Magnetic moment Fourier components	
	(x, y, z)	Circular model $R31'(00\gamma)ts$ Equations (11)–(14)	Elliptical model $R11'(\alpha\beta\gamma)0s$ Equations (15)–(23)
z-plane	Mn1 (9*e*)		
$z = 0$	$(\frac{1}{2}, 0, 0)$	$(u_1, v_1, 0)$	$(u_1, v_1, 0)$
	$(0, \frac{1}{2}, 0)$	$e^{\frac{2}{3}\pi i}(-v_1, u_1 - v_1, 0)$	$(u_1, v_1, 0)$
	$(\frac{1}{2}, \frac{1}{2}, 0)$	$e^{-\frac{2}{3}\pi i}(-u_1 + v_1, -u_1, 0)$	$(u_1, v_1, 0)$
$z = \frac{2}{6}$	$(\frac{1}{6}, \frac{1}{3}, \frac{2}{6})$	$(u_1, v_1, 0)$	$(u_1, v_1, 0)$
	$(\frac{2}{3}, \frac{5}{6}, \frac{2}{6})$	$e^{\frac{2}{3}\pi i}(-v_1, u_1 - v_1, 0)$	$(u_1, v_1, 0)$
	$(\frac{1}{6}, \frac{5}{6}, \frac{2}{6})$	$e^{-\frac{2}{3}\pi i}(-u_1 + v_1, -u_1, 0)$	$(u_1, v_1, 0)$
$z = \frac{4}{6}$	$(\frac{5}{6}, \frac{2}{3}, \frac{4}{6})$	$(u_1, v_1, 0)$	$(u_1, v_1, 0)$
	$(\frac{1}{3}, \frac{5}{6}, \frac{4}{6})$	$e^{\frac{2}{3}\pi i}(-v_1, u_1 - v_1, 0)$	$(u_1, v_1, 0)$
	$(\frac{5}{6}, \frac{1}{6}, \frac{4}{6})$	$e^{-\frac{2}{3}\pi i}(-u_1 + v_1, -u_1, 0)$	$(u_1, v_1, 0)$
z-plane	Mn2 (9*d*)		
$z = \frac{1}{6}$	$(\frac{5}{6}, \frac{1}{6}, \frac{1}{6})$	$e^{i\pi}(u_1, v_1, 0)$	$e^{i\pi}(u_1, v_1, 0)$
	$(\frac{2}{3}, \frac{2}{3}, \frac{1}{6})$	$e^{-\frac{1}{3}\pi i}(-v_1, u_1 - v_1, 0)$	$e^{i\pi}(u_1, v_1, 0)$
	$(\frac{1}{3}, \frac{1}{6}, \frac{1}{6})$	$e^{\frac{1}{3}\pi i}(-u_1 + v_1, -u_1, 0)$	$e^{i\pi}(u_1, v_1, 0)$
$z = \frac{3}{6}$	$(\frac{1}{2}, \frac{1}{2}, \frac{1}{2})$	$e^{i\pi}(u_1, v_1, 0)$	$e^{i\pi}(u_1, v_1, 0)$
	$(\frac{1}{2}, 0, \frac{1}{2})$	$e^{-\frac{1}{3}\pi i}(-v_1, u_1 - v_1, 0)$	$e^{i\pi}(u_1, v_1, 0)$
	$(0, \frac{1}{2}, \frac{1}{2})$	$e^{\frac{1}{3}\pi i}(-u_1 + v_1, -u_1, 0)$	$e^{i\pi}(u_1, v_1, 0)$
$z = \frac{5}{6}$	$(\frac{1}{6}, \frac{5}{6}, \frac{5}{6})$	$e^{i\pi}(u_1, v_1, 0)$	$e^{i\pi}(u_1, v_1, 0)$
	$(\frac{1}{6}, \frac{1}{3}, \frac{5}{6})$	$e^{-\frac{1}{3}\pi i}(-v_1, u_1 - v_1, 0)$	$e^{i\pi}(u_1, v_1, 0)$
	$(\frac{2}{3}, \frac{5}{6}, \frac{5}{6})$	$e^{\frac{1}{3}\pi i}(-u_1 + v_1, -u_1, 0)$	$e^{i\pi}(u_1, v_1, 0)$
z-plane	Mn3 (3*b*)		
$z = \frac{1}{6}$	$(\frac{1}{3}, \frac{2}{3}, \frac{1}{6})$	$(u_3, v_3, 0)$	$(u_3, v_3, 0)$
$z = \frac{3}{6}$	$(0, 0, \frac{3}{6})$	$(u_3, v_3, 0)$	$(u_3, v_3, 0)$
$z = \frac{5}{6}$	$(\frac{2}{3}, \frac{1}{3}, \frac{5}{6})$	$(u_3, v_3, 0)$	$(u_3, v_3, 0)$

$$w_3 = 0. \tag{20}$$

The derivation of equations (15)–(20) is given in the supplementary material.

The amplitudes A_1, B_1 and A_3, B_3 are the half axes of the modulation ellipses for the magnetic moments of Mn1 and Mn3 atoms. The half axis denoted by A_1 (for Mn1) and the half axis denoted by A_3 (for Mn3) are parallel to each other and they both make an angle α with respect to the unit-cell axis **a**. For the specific case of $A_1 = B_1 = M_1$ and $A_3 = B_3 = M_3$ and $\alpha = 0$ one recovers the *circular model* as given by equations (13) and (14). The schematic presentation of the *elliptical model* shown in Fig. 2 is given for $\alpha = 60^\circ$ and $A_1/B_1 = A_3/B_3 = 2$.

The *elliptical model* and the *circular model* give the same neutron powder diffraction patterns when

$$\frac{A_1}{B_1} = \frac{A_3}{B_3} \tag{21}$$

$$A_1^2 + B_1^2 = 2M_1^2 \tag{22}$$

$$A_3^2 + B_3^2 = 2M_3^2. \tag{23}$$

The calculated neutron powder diffraction patterns for the *elliptical model* do not depend on the value of the α angle or on the value of the ellipses deformation half-axes ratio A_1/B_1. In the extreme case of $A_1 = A_3 = 0$ the collinear spin density wave with amplitudes $B_1 = \sqrt{2}M_1$ and $B_3 = \sqrt{2}M_3$ are obtained. It is not possible to decide which model is correct by using neutron powder diffraction data only.

3.3. Neutron powder diffraction data described with the circular model

The neutron powder diffraction pattern of $CaMn_7O_{12}$ (D2B) at 60 K (Sławiński *et al.*, 2010) has been analysed using the crystal structure model given in Bochu *et al.* (1980) and the *circular model* (see §3.2.1) of the magnetic modulation. We refine the ordered magnetic moment amplitudes M_1, M_3 and the modulation vector length q_m. The crystal structure parameters (lattice constants, O1 and O2 positions, individual isotropic Debye–Waller factors for Ca, Mn and O atoms),

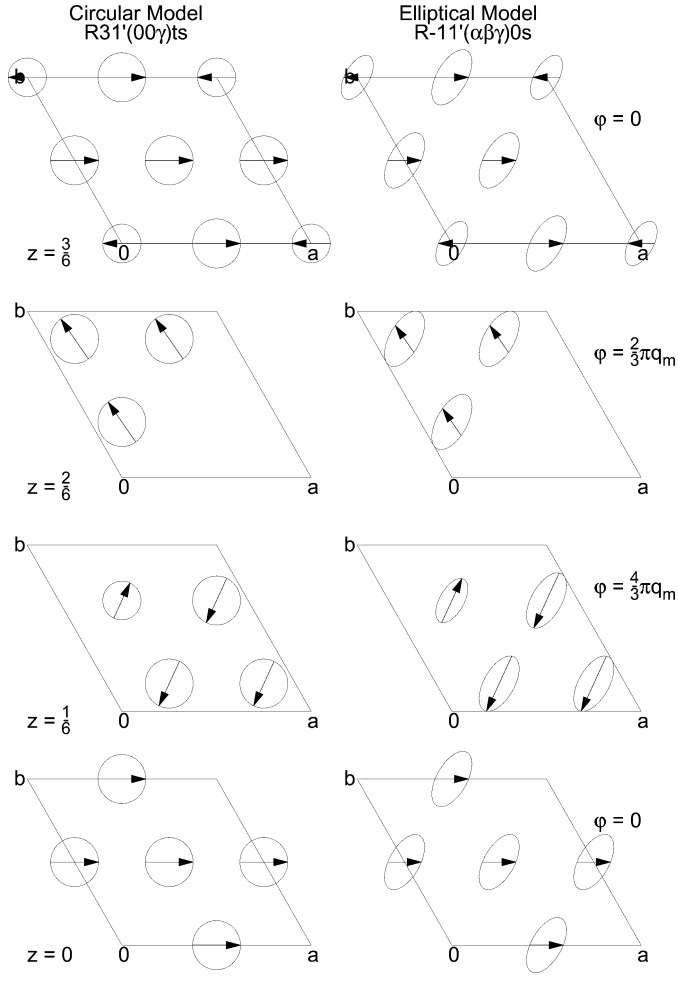

Figure 2
Schematic representation of the *circular model* (left panels) and the *elliptical model* (right panels) of the modulated magnetic ordering in $CaMn_7O_{12}$. The slices of the hexagonal unit cell at constant $z = 0, \frac{1}{6}, \frac{2}{6}$ and $\frac{3}{6}$ coordinates are shown. The longer and shorter arrows represent the ordered magnetic moments of Mn^{3+} and Mn^{4+} ions. The Mn^{3+} and Mn^{4+} ions with the same z coordinate are antiparallel. The directions of the magnetic moments at $z = \frac{4}{6}$ and $z = \frac{5}{6}$ (not shown) can be obtained from Table 7. The φ angle between the Mn^{3+} magnetic moment direction and the *a* axis is indicated for each layer.

Table 8
Magnetic ordering parameters of $CaCu_xMn_{7-x}O_{12}$ compounds determined at T = 60 K using neutron powder diffraction and the circular model of magnetic ordering described with the superspace group $R31'(00\gamma)ts$ with the magnetic modulation vector (0, 0, q_m).

The top lines indicate the instrument and composition parameter x.

Instrument	D2B	D20		
Parameter	x = 0	x = 0	x = 0.1	x = 0.23
M_1 [μ_B]	2.21 (2)	2.27 (3)	1.87 (2)	1.02 (2)
M_3 [μ_B]	1.95 (5)	1.91 (7)	1.66 (3)	0.86 (7)
q_m[c^*]	1.0391 (3)	1.0403 (6)	1.0479 (3)	1.0528 (16)
L_m (Å)	162.1 (1.2)	157.3 (2.5)	132.6 (1.0)	119.9 (3.7)
a (Å)	10.4452 (2)	10.4372 (11)	10.4312 (13)	10.4032 (20)
c (Å)	6.3453 (1)	6.3414 (9)	6.3417 (9)	6.3340 (14)

peak-width parameters (U, V, W), peak-shape parameters (pseduo-Voigt: Gauss U, V, W and Lorentz Lx and Ly), zero-shift parameter, background (30 terms Legendre polynomials), absorption correction (cylindrical sample) and asymmetry (divergence S/L = H/L parameter) has been refined. The refinements were performed using the program *JANA*2006 (Petříček *et al.*, 2006). The resulting fit gives good agreement with the experimental data, as shown in Fig. 3. The values of the refined parameters are given in Table 8. The magnetic modulation length L_m is calculated as $L_m = c/(q_m - 1)$.

Refinement of the neutron powder diffraction patterns of $CaCu_xMn_{7-x}O_{12}$, x = 0, 0.1 and 0.23, measured earlier with a D20 (λ = 2.418 Å) instrument at 60 K (Sławiński *et al.*, 2010) was also carried out. Refinements with the *circular model* of magnetic ordering are shown in Figs. 4(*a*), (*b*) and (*c*) for $CaCu_xMn_{7-x}O_{12}$, x = 0, 0.1 and 0.23. The values of the refined parameters are given in Tables 8 and 9. The temperature dependence of the magnetic moment amplitudes M_1, M_3 is shown in Fig. 5. The temperature dependence of the modulation vector length q_m is shown in Fig. 6. The Néel temperatures for $CaCu_xMn_{7-x}O_{12}$, x = 0, 0.1 and 0.23 are estimated as: 90.4, 89.2 and 78.1 K (Sławiński *et al.*, 2009).

The magnetic ordering parameters obtained for $CaMn_7O_{12}$ at 60 K from D2B data (all magnetic peaks – see Fig. 3) and from D20 data (see Fig. 4) agree within statistical error, as shown in Table 8.

Our present results should be compared with the results of Johnson *et al.* (2012). The authors of Johnson *et al.* (2012) use a different equivalent modulation vector $(0, 1, 2 - q)$ and different restrictions of magnetic moments, but still within the same representation that we use. The values of the magnetic modulation amplitudes determined by Johnson *et al.* (2012) at 65 K are similar to our results shown in Table 8. As mentioned above our circular model is based on fixed relative phases between Mn2/Mn1 and Mn3/Mn1 helicoids. Their deviations from idealized values as refined from our experimental data set were not significant and moreover the restricted model gives a more symmetrical solution (see Fig. 1). The authors of Johnson *et al.* (2012) did not take into account the modulation of the atomic positions in $CaMn_7O_{12}$ and they also did not discuss the coupling between the positional and magnetic modulations.

Between 50 and 70 K the values of q_m are constant and equal to 1.045 (11), 1.050 (7) and 1.053 (2) corresponding to magnetic modulation lengths $L_m = c/(q_m - 1)$ equal to 155 (2), 132 (3) and 120 (5) Å for $CaCu_xMn_{7-x}O_{12}$, x = 0, 0.1 and 0.23, respectively. The values of q_m tend to increase when approaching T_N.

Both *the circular* and *the elliptical models* give no net magnetic moment, while the ferrimagnetic ordering described for $CaMn_7O_{12}$ (Przeniosło *et al.*, 1999) gave a relatively large net sum of 9.25 μ_B for all the magnetic moments in the hexagonal unit cell of $CaMn_7O_{12}$ (0.44μ_B per Mn ion). The absence of a large net ferromagnetic contribution is in agreement with recent literature (Zhang *et al.*, 2011; Johnson *et al.*, 2012).

The most intense magnetic peaks were indexed as $(h, k, 0)$ (Przeniosło *et al.*, 1999) and they were ascribed as the ferrimagnetic phase. In the present model these peaks are indexed as $(h, k, 1 - q_m)$. Due to the small value of $1 - q_m \simeq -0.04$, the difference between the 2θ positions of $(h, k, 0)$ and $(h, k, 1 - q_m)$ was smaller than the experimental accuracy in the paper (Przeniosło *et al.*, 1999). It is important to stress that the

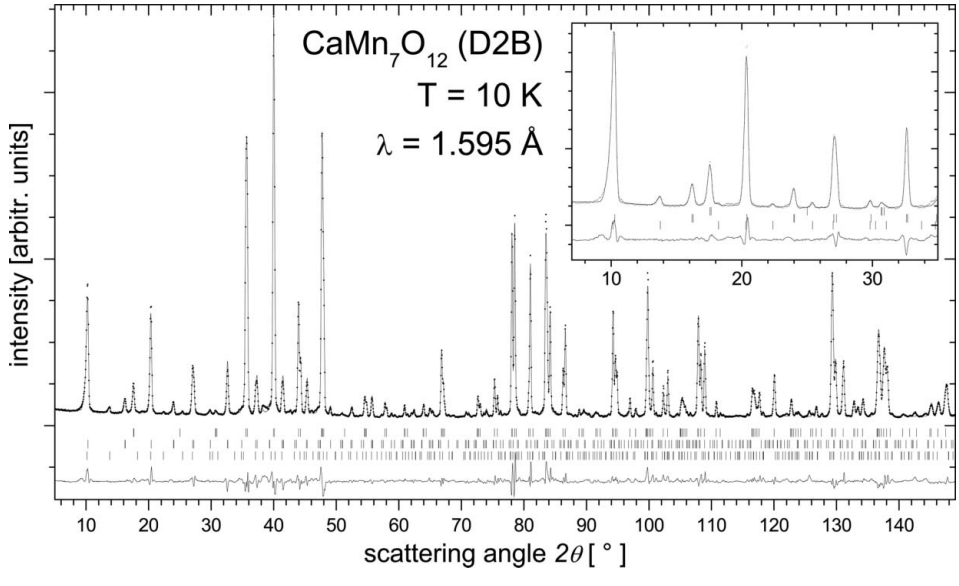

Figure 3
Rietveld plot of the neutron powder diffraction pattern (λ = 1.595 Å) of $CaMn_7O_{12}$ measured at 60 K. Solid points = measured data, solid line through the data points = refined profile, solid line at bottom = difference. The sets of tick marks represent the Bragg positions for $CaMn_7O_{12}$ (top) crystal structure and $CaMn_7O_{12}$ magnetic structure (bottom). The insert shows the enlarged part of the pattern for low scattering angles.

ferrimagnetic ordering proposed in Przeniosło *et al.* (1999) is no longer valid.

The temperature dependence of the magnetic contributions observed for $CaCu_xMn_{7-x}O_{12}$ near T_N are shown in Figs. 7(*a*) and (*b*). For $CaCu_xMn_{7-x}O_{12}$, $x = 0.1$, the difference patterns are taken as $I(T) - I(107\,K)$ (see Fig. 7*a*), while for $CaCu_xMn_{7-x}O_{12}$, $x = 0.23$, it is $I(T) - I(92\,K)$ (see Fig. 7*b*). The narrow magnetic Bragg peaks $(1, 0, 1 - q_m)$ and $(2, 0, 1 - q_m)$ decrease and transform to broad features at higher temperature. This is an indication of the magnetic short-range order which persists up to ~ 15 K above T_N. A similar effect over a larger temperature scale was observed in β-MnO_2 (Regulski *et al.*, 2004).

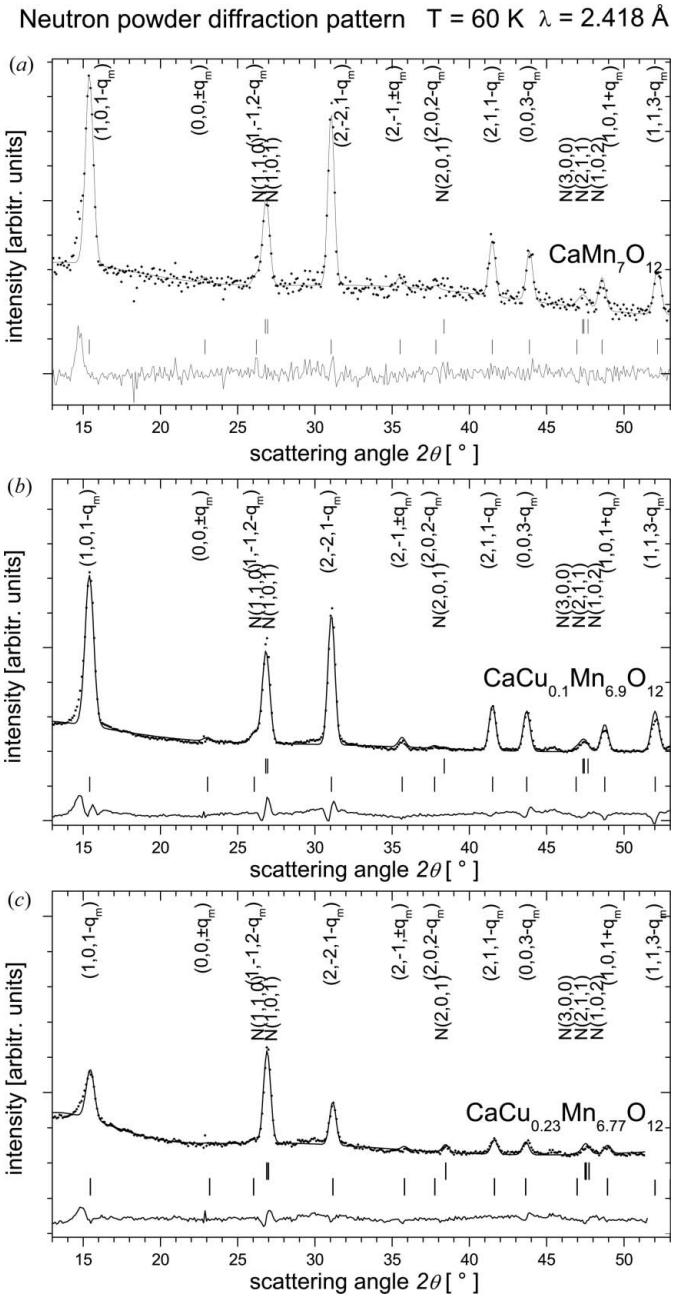

Figure 4
Parts of the Rietveld refinement plots of neutron powder diffraction patterns (ILL D20, λ = 2.418 Å) measured at 60 K for $CaCu_xMn_{7-x}O_{12}$, for $x = 0.0$ (panel *a*), 0.1 (panel *b*) and 0.23 (panel *c*). Solid points = measured data, solid line through the data points = refined profile, solid line at bottom = difference. The two sets of tick marks represent the Bragg positions for $CaMn_7O_{12}$ crystal structure (top) and $CaMn_7O_{12}$ magnetic structure (bottom).

4. Conclusions

The atomic position modulation and the magnetic modulation in $CaCu_xMn_{7-x}O_{12}$ can be quantitatively described with one

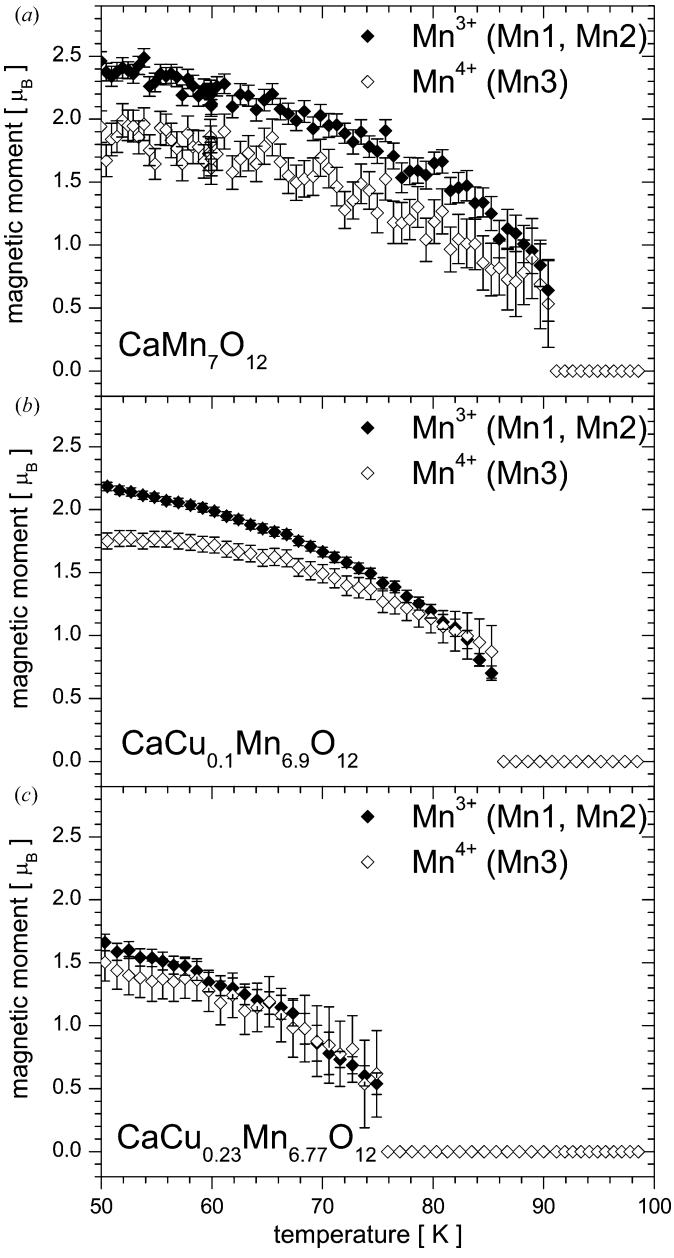

Figure 5
Temperature dependence of the ordered magnetic moments of Mn^{3+} and Mn^{4+} ions in $CaCu_xMn_{7-x}O_{12}$, where $x = 0.0$ (panel *a*), 0.1 (panel *b*) and 0.23 (panel *c*), as determined from Rietveld refinement of neutron powder diffraction data (instrument D20).

Table 9
Summary of crystal and experimental data.

Chemical formula	$CaMn_7O_{12}$	$CaMn_7O_{12}$	$CaCu_{0.1}Mn_{6.9}O_{12}$	$CaCu_{0.23}Mn_{6.77}O_{12}$
Space group (crystal structure)	$R\bar{3}$ (No. 148)	$R\bar{3}$ (No. 148)	$R\bar{3}$ (No. 148)	$R\bar{3}$ (No. 148)
Superspace group (magnetic structure)	$R31'(00\gamma)ts$	$R31'(00\gamma)ts$	$R31'(00\gamma)ts$	$R31'(00\gamma)ts$
Temperature (K)	60.0	60.0	60.7	60.7
a, b, c (Å)	10.4452 (2), 10.4452 (2), 6.3453 (1)	10.4372 (11), 10.4372 (11), 6.3414 (9)	10.4312 (13), 10.4312 (13), 6.3417 (9)	10.4032 (20), 10.4032 (20), 6.3340 (14)
V (Å^3)	599.54 (2)	598.2 (1)	597.6 (1)	593.6 (7)
Z	6	6	6	6
Number of main reflections ($m = 0$)	260	74	74	72
Number of satellite reflections ($\|m\| = 1$)	528	156	152	152
$(\sin\theta/\lambda)_{max}$	0.617	0.389	0.389	0.389
D_x (g cm^{-3})	5.1220 (2)	5.133 (1)	5.147 (2)	5.190 (2)
λ (Å)	1.595	2.418	2.418	2.418
Diffractometer	ILL D2B	ILL D20	ILL D20	ILL D20
Method of measurement	Debye–Scherrer	Debye–Scherrer	Debye–Scherrer	Debye–Scherrer
Modulation vector	$\mathbf{q}_m = 1.0391\ (3)\mathbf{c}^*$	$\mathbf{q}_m = 1.0403\ (6)\mathbf{c}^*$	$\mathbf{q}_m = 1.0479\ (3)\mathbf{c}^*$	$\mathbf{q}_m = 1.0528\ (16)\mathbf{c}^*$
Refinement method	*JANA*2006	*JANA*2006	*JANA*2006	*JANA*2006

model based on the magnetic superspace group $R31'(00\gamma)ts$ (so-called circular model of magnetic ordering). This model seems to be more appropriate from the symmetry point of view and it might be used in further investigations of the interactions which lead to the multiferroic properties of $CaCu_xMn_{7-x}O_{12}$ compounds.

It is, however, important to note that this model has not been unambiguously determined. Our experimental neutron diffraction data can be equally well described with a family of *elliptical models* of the magnetic ordering described with the superspace group $R11'(\alpha\beta\gamma)0s$. A similar ambiguity was discussed in the case of another distorted perovskite $BiFeO_3$ (Przeniosło *et al.*, 2006).

The atomic position modulation could also be described with another model based on the superpsace group $R31'(00\gamma)0s$. These ambiguities motivate further diffraction studies with $CaMn_7O_{12}$ single crystals.

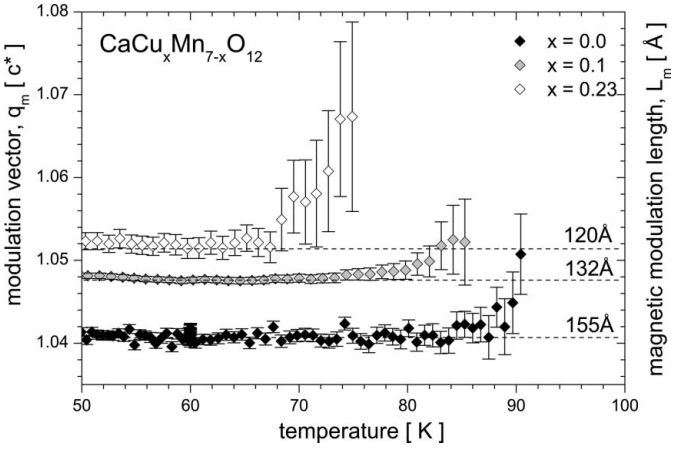

Figure 6
Temperature dependence of the magnetic modulation propagation vector length q_m for $CaCu_xMn_{7-x}O_{12}$, where $x = 0.0$, 0.1 and 0.23, determined from Rietveld refinement of neutron powder diffraction data (instrument D20).

Thanks are due to E. Suard (ILL) and M. Bieringer (University of Manitoba) for help in the neutron diffraction measurements and sample preparation. We are grateful to the ILL for providing beamtime. Thanks are due to the Ministry of Science and Higher Education (Poland) for the research projects No. IP 2010 038070 and 2011/01/B/ST3/02401 and for providing access to the ILL (project 458/1/N-ILL/2010/0). VP was supported by the Praemium Academiae.

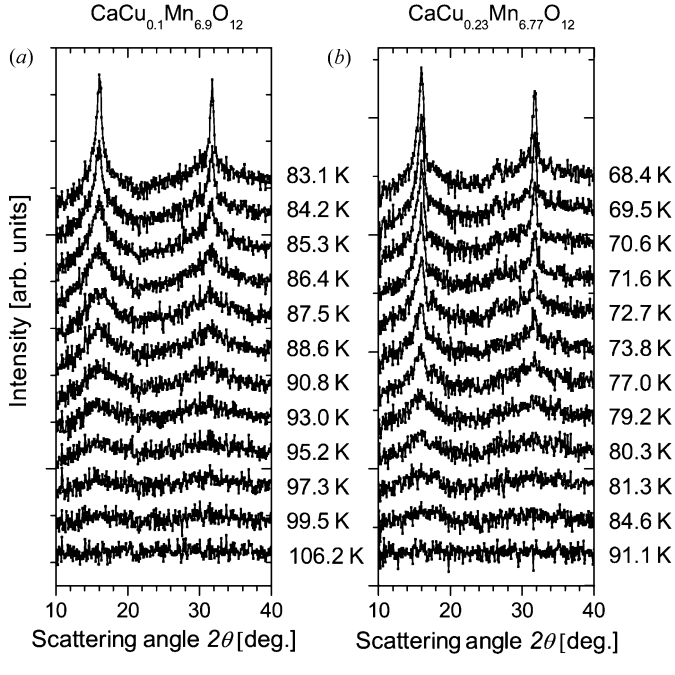

Figure 7
Temperature changes of the magnetic contributions to the neutron powder diffraction patterns of $CaCu_xMn_{7-x}O_{12}$, where $x = 0.1$ (panel *a*) and $x = 0.23$ (panel *b*) measured in the vicinity of the Néel temperature. The magnetic contributions are calculated as $I(T) - I(107\ \text{K})$ for $x = 0.1$ and $I(T) - I(92\ \text{K})$ for $x = 0.23$.

References

Bochu, B., Buevoz, J., Chenavas, J., Collomb, A., Joubert, J. & Marezio, M. (1980). *Solid State Commun.* **36**, 133–138.

Campbell, B. J., Stokes, H. T., Tanner, D. E. & Hatch, D. M. (2006). *J. Appl. Cryst.* **39**, 607–614.

Dagotto, E., Hotta, T. & Moreo, A. (2001). *Phys. Rep.* **344**, 1–153.

Fiebig, M. (2005). *J. Phys. D Appl. Phys.* **38**, R123–R152.

Johnson, R. D., Chapon, L. C., Khalyavin, D. D., Manuel, P., Radaelli, P. G. & Martin, C. (2012). *Phys. Rev. Lett.* **108**, 067201.

Katsura, H., Nagaosa, N. & Balatsky, A. V. (2005). *Phys. Rev. Lett.* **95**, 057205.

Kim, J. *et al.* (2008). *Phys. Rev. B*, **78**, 245115

Kimura, T., Sekio, Y., Nakamura, H., Siegrist, T. & Ramirez, A. P. (2008). *Nat. Mater.* **7**, 291–294.

Lee, S., Choi, T., Ratcliff, W., Erwin, R., Cheong, S. W. & Kiryukhin, V. (2008). *Phys. Rev. B*, **78**, 100101.

Lunkenheimer, P., Krohns, S., Riegg, S., Ebbinghaus, S. G., Reller, A. & Loidl, A. (2010). *Eur. Phys. J.* **180**, 61–89.

Mostovoy, M. (2006). *Phys. Rev. Lett.* **96**, 067601.

Perez-Mato, J. M., Ribeiro, J. L., Petricek, V. & Aroyo, M. I. (2012). *J. Phys. Condensed Matter*, **24**, 163201.

Petříček, V., Dušek, M. & Palatinus, L. (2006). *JANA*2006. Institute of Physics, Praha, Czech Republic.

Petříček, V., Fuksa, J. & Dušek, M. (2010). *Acta Cryst.* A**66**, 649–655.

Przeniosło, R., Regulski, M. & Sosnowska, I. (2006). *J. Phys. Soc. Jpn*, **75**, 084718.

Przeniosło, R., Sosnowska, I., Hohlwein, D., Hauss, T. & Troyanchuk, I. O. (1999). *Solid State Commun.* **111**, 687–692.

Przeniosło, R., Sosnowska, I., Suard, E., Hewat, A. & Fitch, A. N. (2004). *Physica B*, **344**, 358–367.

Regulski, M., Przeniosło, R., Sosnowska, I. & Hoffmann, J. (2004). *J. Phys. Soc. Jpn*, **73**, 3444–3447.

Rietveld, H. M. (1969). *J. Appl. Cryst.* **2**, 65–71.

Rodríguez-Carvajal, J. (1993). *Physica B*, **192**, 55–69.

Sánchez-Andújar, M., Yáñez-Vilar, S., Biskup, N., Castro-García, S., Mira, J., Rivas, J. & Señarís-Rodríguez, M. A. (2009). *J. Magn. Magn. Mater.* **321**, 1739–1742.

Sławiński, W., Przeniosło, R., Sosnowska, I. & Bieringer, M. (2010). *J. Phys. Condens. Matter*, **22**, 186001.

Sławiński, W., Przeniosło, R., Sosnowska, I., Bieringer, M., Margiolaki, I., Fitch, A. N. & Suard, E. (2006). *J. Solid State Chem.* **179**, 2443–2451.

Sławiński, W., Przeniosło, R., Sosnowska, I., Bieringer, M., Margiolaki, I. & Suard, E. (2009). *Acta Cryst.* B**65**, 535–542.

Sosnowska, I., Neumaier, T. P. & Steichele, E. (1982). *J. Phys. Solid State Phys.* **15**, 4835–4846.

Stokes, H. T., Campbell, B. J. & van Smaalen, S. (2011). *Acta Cryst.* A**67**, 45–55.

Vasiliev, A. N. & Volkova, O. S. (2007). *Fiz. Nizk. Temp. (Kharkov)*, **33**, 1181–1205.

Volkova, O., Arango, Y., Tristan, N., Kataev, V., Gudilin, E., Meier, D., Lorenz, T., Buchner, B. & Vasil'ev, A. (2005). *JETP Lett.* **82**, 444–446.

Wang, K. F., Liu, J. & Ren, Z. F. (2009). *Adv. Phys.* **58**, 321–448.

Yamasaki, Y., Sagayama, H., Goto, T., Matsuura, M., Hirota, K., Arima, T. & Tokura, Y. (2007). *Phys. Rev. Lett.* **98**, 147204.

Yáñez-Vilar, S., Castro-Couceiro, A., Rivas-Murias, B., Fondado, A., Mira, J., Rivas, J. & Sēnarís-Rodríguez, M. A. (2005). *Z. Anorg. Allg. Chem.* **631**, 2265–2272.

Zeng, Z., Greenblatt, M., Sunstrom, J. E., Croft, M. & Khalid, S. (1999). *J. Solid State Chem.* **147**, 185–198.

Zhang, G., Dong, S., Yan, Z., Zhang, Q., Yunoki, S., Dagotto, E. & Liu, J.-M. (2011). *Phys. Rev. B*, **84**, 174413.